

Constraining the shape of the CMB: a Peak-by-Peak analysis.

Carolina J. Ödman[‡], Alessandro Melchiorri[‡], Michael P. Hobson[‡] and Anthony N. Lasenby[‡]

[‡] *Astrophysics Group, Cavendish Laboratory, Cambridge University, Cambridge, U.K.*

[‡] *Astrophysics, Denys Wilkinson Building, University of Oxford, Keble road, OX1 3RH, Oxford, UK*

The recent measurements of the power spectrum of Cosmic Microwave Background anisotropies are consistent with inflationary initial conditions for structure formation and big bang nucleosynthesis constraints. However, these results rely on the assumption of a class of models based on primordial adiabatic perturbations, cold dark matter and a cosmological constant. In this paper we investigate the need for deviations from the Λ -CDM scenario by first characterizing the peaks in the spectrum using different phenomenological functions in a 15 dimensional parameter space. Using a Monte Carlo Markov chain approach to Bayesian inference and a low curvature model template we then check for the presence of new physics and/or systematics in the CMB data. We find an almost perfect consistency between the data and the theory. However, the curvature of the secondary peaks is weakly constrained by the present data. The improved spectral resolution expected from future satellite experiments is clearly warranted for a definitive test of the scenario.

I. INTRODUCTION.

The recent observational evidence for multiple peaks in the cosmic microwave background (CMB) power spectrum ([1], [2], [3], [4], [5], [6], [7]) have presented cosmologists with the possibility of studying the large scale properties of our universe with unprecedented precision. As is well known (see e.g. [8]), the structure of the CMB spectrum, given mainly by the relative positions and amplitude of the peaks, is sensitive to several cosmological parameters. The existing CMB datasets are therefore being analyzed with increasing sophistication (see [9] and [10] for important advancements) in an attempt to measure the undetermined cosmological quantities. The most recent analyses of this kind ([11], [12], [13], [14], [15], [16], [43], [18]) have revealed an outstanding agreement between the data and the inflationary predictions of a flat universe and of a primordial scale invariant spectrum of adiabatic density perturbations. Furthermore, the CMB constraint on the amount of matter density in baryons, ω_b , is now in very good agreement with the independent constraints from standard big bang nucleosynthesis (BBN) (see e.g. [17]). Finally, the detection of power around the expected third peak, on arc-minutes scales, provides a new and independent evidence for the presence of non-baryonic dark matter ([18]).

The actual data is therefore suggesting that our present cosmological model represents a beautiful and elegant theory able to explain most of the observations.

However, the CMB result relies on the assumption of a particular class of models, based on adiabatic, *passive* and *coherent* (see [26]) primordial fluctuations, and cold dark matter. In the following we will refer to this class of model as Λ -Cold Dark Matter (Λ -CDM).

This weak point, shared by most of the current studies, should not be overlooked: it has been recently shown, for example, that the very legitimate inclusion

of gravity waves (see e.g. [38]) or isocurvature modes ([19], [40], [20]) into the analysis can completely erase most of the constraints derived from CMB alone.

Furthermore, since even more exotic modifications like quintessence ([23]), topological defects ([34], [21]), broken primordial scale invariances ([39], [24], [25]), extra dimensions ([35]) or unknown systematics (just to name a few) can be in principle considered, one should be extremely cautious in taking any definitive conclusion from the present CMB observations.

It is therefore timely to investigate if the actual CMB data is in complete agreement with the Λ -CDM scenario or if we are losing relevant scientific informations by restricting the current analysis to a subset of models (see e.g. [27]).

In the present *paper* we check to what extent modifications to the standard Λ -CDM scenario are *needed* by current CMB observations with two complementary approaches: First, we provide a model-independent analysis by fitting the actual data with a phenomenological function and characterizing the observed multiple peaks. Phenomenological fits have been extensively used in the past and recent CMB analyses ([28], [29], [30], [41]). Our analysis differs in two ways: we include the new data from the VSA and CBI experiments and we make use of a Monte Carlo Markov Chain (MCMC) algorithm, which allows us to investigate a large number of parameter simultaneously (15 in our case).

We then compare the position, relative amplitude and width of the peaks with the same features expected in a 4-parameters model template of Λ -CDM spectra. By doing a peak-by-peak comparison between the theory and the phenomenological fit which is based on a much wider set of parameters, we then verify in a systematic way the agreement with the standard theoretical expectations.

As a by-product of the analysis, we present a set of cosmological diagrams that directly translate, under the assumption of Λ -CDM, the constraints on the

features in the spectrum into bounds on several cosmological parameters. These diagrams offer the opportunity of quick, by-eye, data to model comparison.

Our paper is organized as follows: In section II we discuss the phenomenological representation of the power spectrum, the analysis method we used and the MCMC algorithm. In section III we present our results. Finally, in section IV, we discuss our conclusions.

II. PHENOMENOLOGICAL REPRESENTATION.

We model the multiple peaks in the CMB angular spectrum by the following function:

$$\ell(\ell+1)C_\ell/2\pi = \sum_{i=1}^N \Delta T_i^2 \exp(-(\ell - \ell_i)^2/2\sigma_i^2) \quad (1)$$

where, in our case, $N = 5$. We use this formula to make a phenomenological fit to the current CMB data, constraining the values of the 15 parameters ΔT_i , ℓ_i and σ_i .

The use of gaussian-shaped function to describe the CMB spectrum is now becoming a standard method in the literature (see e.g. [29], [30], [11], [15]). As a major difference with respect to previous works, we note that we are using only *one* fitting function, varying *simultaneously* all its parameters, while in general different fits are made with one single gaussian in different selected regions of the spectrum, in correspondance with the expected peaks.

Recently, Douspis and Ferreira ([41]) used as phenomenological model a Gaussian function plus an oscillating function. The method used here is more general, in the sense that we allow for independent amplitudes and widths of the secondary peaks.

For the CMB data, we use the recent results from the BOOMERanG-98, DASI, MAXIMA-1, CBI, and VSA experiments. The power spectra from these experiments were estimated in 19, 9, 13, 14 and 10 bins respectively (for the CBI, we use the data from the MOSAIC configuration), spanning the range $2 \leq \ell \leq 3500$. However, since in this work we are interested only in comparing the data with the expected *primary* anisotropies, we limit our analysis to the region $\ell < 1500$ which is likely not to be affected by secondary effects like Sunyaev-Zel'dovich (see e.g. [36]). For the DASI, MAXIMA-I and VSA experiments we use the publicly available correlation matrices and window functions. For the BOOMERanG and CBI experiments we assign a flat interpolation for the spectrum in each bin $\ell(\ell+1)C_\ell/2\pi = C_B$, and we approximate the signal C_B inside the bin to be a Gaussian variable. The likelihood for a given phenomenological model is defined by $-2\ln\mathcal{L} = (C_B^{ph} - C_B^{ex})M_{BB'}(C_B^{ph} - C_B^{ex})$

where $M_{BB'}$ is the Gaussian curvature of the likelihood matrix at the peak.

We discard the first bin of the CBI dataset ($0 < \ell < 400$), due to the asymmetric window function and the high sample variance.

We consider 10%, 4%, 5%, 7% and 5% Gaussian distributed calibration errors for the BOOMERanG-98, DASI, MAXIMA-1, VSA, and CBI experiments respectively and we include the beam uncertainties by the analytical marginalization method presented in ([31], [44]).

We perform our analysis on three sets of CMB data. We first compare our results without the recent interferometer data, to those obtained including the VSA and CBI results. Secondly, since CBI is the only experimental data above $\ell \sim 1200$, we test the stability of our result in that region repeating the analysis with the two different CBI binnings as described in [6].

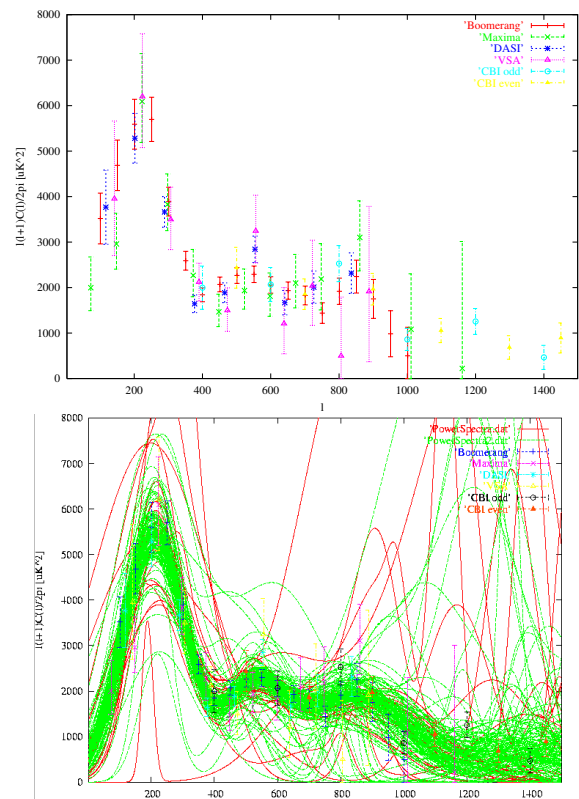


FIG. 1. Upper panel: The CMB data used in this analysis: beam and calibration errors are not included. Lower panel: The red curves are a set of phenomenological power spectra generated during the burn-in period of the MCMC routine. The green spectra are generated after burn-in, when the MCMC algorithm has found the most likely regions in parameter space. The few very unrealistic spectra show how wide a parameter space we investigated.

The phenomenological fit is operated through a MCMC algorithm. The MCMC approach is to generate a random walk through parameter space that converges towards the most likely value of the parameters and samples the parameter space following the joint

likelihood, the posterior probability distribution. In the general case, the number of parameters and their priors have to be defined. There is no limit in resolution (except numerical precision of the computer). The priors define the volume in parameter space in which the random walk will take place.

At each iteration, a point \mathbf{x}_{n+1} is randomly selected in the m -dimensional parameter space. Its likelihood is evaluated by comparing to data. A sample is said to be accepted into the Markov chain or not, depending on the following acceptance criterion:

$$u \leq \min \left\{ 1, \frac{p(\mathbf{x}_{n+1})\mathcal{L}(\mathbf{x}_{n+1})}{p(\mathbf{x}_n)\mathcal{L}(\mathbf{x}_n)} \right\}, \quad (2)$$

where u is a random number sampled from a uniform distribution on the interval $[0, 1]$, $p(\mathbf{x})$ is the prior, and $\mathcal{L}(\mathbf{x})$ is the likelihood, containing the information from the data. During an initial period, called the burn-in, the random walk simply makes its way through parameter space and converges towards the maximum likelihood. Then, it samples parameter space (see Fig. 1). At the end of the MCMC routine, the samples are counted and their density onto one or more dimensions represents the marginalised posterior distribution of the parameters. The posterior probability of the parameter value is proportional to the density of samples at that value. If the posterior follows a gaussian distribution, the best fit value is obtained by averaging over the samples. The MCMC procedure is described in more detail in [43].

In order to avoid degeneracy of overlapping gaussians, we parametrise the centers of the secondary gaussians as functions of the positions of the previous gaussians:

$$\begin{aligned} l_2 &= l_1(1 + \alpha) \\ l_3 &= l_1(1 + \alpha + \beta) \\ l_4 &= l_1(1 + \alpha + \beta + \gamma) \\ l_5 &= l_1(1 + \alpha + \beta + \gamma + \delta) \end{aligned} \quad (3)$$

We used wide uniform priors for each parameter, in which our resulting likelihoods are fully encompassed, except for ΔT_5 , σ_3 , σ_4 and σ_5 which are not fully constrained from the data. We ran the MCMC routine in order to get ~ 5000 samples for each data set.

We then considered a flat, adiabatic, Λ -CDM model template of CMB angular power spectra, computed with CMBFAST ([32]), sampling the various parameters as follows: $\Omega_{cdm}h^2 \equiv \omega_{cdm} = 0.01, \dots, 0.40$, in steps of 0.01; $\Omega_b h^2 \equiv \omega_b = 0.001, \dots, 0.040$, in steps of 0.001 and $\Omega_\Lambda = 0.0, \dots, 0.95$, in steps of 0.05. The value of the Hubble constant is not an independent parameter, since:

$$h = \sqrt{\frac{\omega_{cdm} + \omega_b}{1 - \Omega_\Lambda}}. \quad (4)$$

We vary the spectral index of the primordial density perturbations within the range $n_s = 0.60, \dots, 1.40$ (in steps of 0.02).

For each model in the template we then consider the corresponding values ΔT_i , ℓ_i , σ_i such that the formula in Eq. (1) represents the best fit to its shape. We found that, restricting the range in ℓ to 50, ..., 1500, equation (1) can well approximate (better than $\sim 10\%$ in C_ℓ) the shape of the spectra in our template.

We also checked that the use of different phenomenological functions such as, for example, Lorentzians or log-normals instead of Gaussians, has no relevant effect on our results.

It is important to note that we have restricted our template of theoretical models to a set of only 4 parameters. However, because of the 'cosmic-degeneracy', this is enough to describe the possible shapes of the CMB spectra in the Λ -CDM scenario. Increasing the optical depth τ_c or adding a gravity waves background, for example, is nearly equivalent to changing some of the parameters already considered like n_s and ω_b . On the other hand we characterize the peaks in the spectrum with a phenomenological fit based on 15 parameters, which allows for independent positions, amplitudes and widths of the observed features.

The comparison between the model-independent values ΔT_i , ℓ_i and σ_i obtained by fitting the data with Eq. (1) and the corresponding values expected in the template of theoretical models represents therefore a strong check of the theory and can give hints for the presence of systematics and/or new physics.

III. RESULTS

In Table I we report the 68% limits on ΔT_i , ℓ_i and σ_i of Eq. 1 obtained by analyzing the present CMB data with an MCMC procedure for each subset of CMB data. We also report the constraints on combinations of those parameters that are more directly connected to the cosmological parameters (see the discussion below).

Figure 2 shows the marginalised likelihood functions of the important CMB observables, and the agreement between the three data subsets. Figure 3 shows the best-fit cosmological and phenomenological models. Although our sums of gaussians comprises any cosmological power spectrum to within 10%, their preferred shape differs from the cosmological model, especially at ℓ greater than ~ 1000 . This is due to the large parameter space allowing to fit the data very well, and appears when comparing the results from analyzing three different sets of data. In this range, more experimental data, or stronger priors are needed to infer reasonable constraints.

The values are in reasonable agreement with the results obtained by similar analysis (see e.g. [11], [30], [41], [15]) and clearly point towards the presence of multiple peaks in the data.

The confidence levels plotted in figure 4 show that by constraining three peaks simultaneously, we obtain

tighter constraints on their shapes and positions than in previous studies.

The positions and amplitudes of the first three peaks seem now well constrained (see Table 1). However, due to the beam systematics and to the current experimental spectral resolution ($\Delta\ell \sim 50$ at best), the *width* of the secondary peaks does not appear to be strongly constrained.

The inclusion of the CBI and VSA data, while fully consistent with the previous results, does not drastically improve the detection of the second and third peak, as the very small variations of the phenomenological fits also show on those scales (see Fig.3).

The CBI data at high ℓ is in agreement with the expected damping tail (see e.g. [50]). However, again, the poor spectral resolution ($\Delta\ell \sim 200$) does not allow us to constrain subsequent peaks or to differentiate them from simple step functions or spikes in the data (see in particular the case of the CBI “odd” binning”).

Still, it is interesting to compare the values obtained with those expected in the Λ -CDM scenario and using priors, as we do in the last three columns of Table 1 (see caption).

Generally speaking, considering that the reported errors are at $1\text{-}\sigma$ and that the theoretical models are COBE normalized, which allows for a further 10% shift in amplitude, the predicted and observed values appear in very good agreement.

It is, however, interesting to notice that the subsequent peaks appear to be lower in amplitude than those expected in the concordance model with $n_s = 1$. This favors a spectral index n_s slightly lower than one, as we will see. However, as is well known, there is a strong degeneracy between n_s and the optical depth τ_c (see e.g. [13]) and models with $n_s = 1$ can be put in better agreement with the observations by an increase in τ_c .

We further investigated the consistency with Λ -CDM by considering phenomenological diagrams relating the relative amplitudes and positions of the peaks with variations in a specific physical parameter.

In the Λ -CDM adiabatic scenario, two key parameters control the relative power between the first and second peaks: the physical baryon density ω_b and the primordial spectral index n_s (see e.g. [42]). Increasing ω_b enhances the odd-numbered peaks relative to the even-numbered ones, while increasing n_s enhances the small-scale peaks relative to the ones at larger scales.

In figure 5 we have plotted the values allowed in our model template (restricted by a set of rather conservative cosmological constraints, see the caption in the figure) for the relative amplitude $\Delta T_1/\Delta T_2$ as functions of the parameters ω_b and n_s . As expected, increasing (decreasing) ω_b (n_s) increases $\Delta T_1/\Delta T_2$.

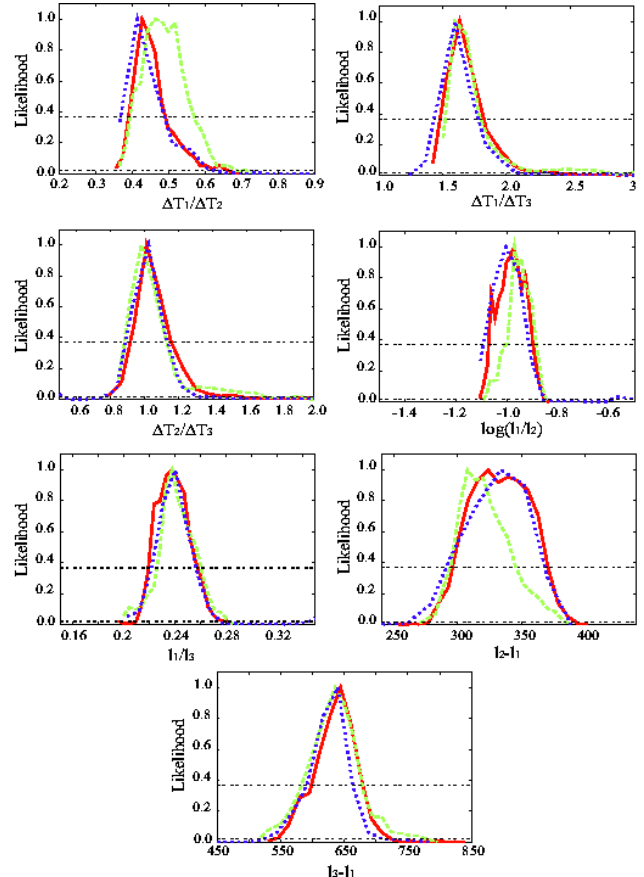


FIG. 2. Marginalised likelihood functions for CMB observables. The red (solid), green (dashed) and blue (dotted) curves correspond to the following three data sets, respectively: without VSA and CBI data, using VSA and CBI even binning, using VSA and CBI odd binning.

Mainly due to the degeneracy between these two parameters, the region is very broad. However, superimposing the $1\text{-}\sigma$ constraint on $\Delta T_1/\Delta T_2$ in the diagram, can provide interesting constraints. Models with a value of the spectral index $n_s > 1.15$, not easily accommodated in most of the inflationary models (see e.g. [45] and references therein), or in disagreement with the BBN constraint $\omega_b = 0.020 \pm 0.002$, are in fact not favored by the observational value. In the figure, we have also plotted the constraints obtained by fitting the CMB data with the models in the template. As we can see, this reduces in a severe way the number of the allowed Λ -CDM models, however the result on the relative amplitude of the peaks is completely consistent with the one derived by the phenomenological fit.

This method can provide better constraints on the amount of cold dark matter ω_{cdm} if we consider the relative amplitudes $\Delta T_1/\Delta T_3$ and $\Delta T_2/\Delta T_3$ as we do in the top and bottom panels of figure 6. A decrease in ω_{cdm} has the effect of decreasing the amplitude of the third peak (see e.g. [46]). As we can see, the two observational values of $\Delta T_1/\Delta T_3$ and $\Delta T_2/\Delta T_3$ provide in a non trivial way similar constraints on ω_{cdm} .

TABLE I. First 3 columns: $1\text{-}\sigma$ constraints on the parameters of the phenomenological model for three different observational sets of data. The range for the same parameters in a database of COBE normalized theoretical models (no CMB data is considered) is also reported in the next 2 columns for the case of *weak* priors ($0.05 < \Omega_{\text{cdm}} < 0.5$, $0.15 < \Omega_b h^2 < 0.25$, $0.55 < h < 0.88$, $0.80 < n_s < 1.10$) and *strong* priors ($0.10 < \Omega_{\text{cdm}} < 0.35$, $0.18 < \Omega_b h^2 < 0.22$, $0.65 < h < 0.80$, $0.95 < n_s < 1.05$). In the last column we also show the values for a COBE normalized *concordance* model with $\Omega_{\text{cdm}} = 0.31$, $\Omega_b = 0.04$, $h = 0.7$ and $n_s = 1$.

CMB Observable	w/o VSA and CBI Phen. Fit	+ VSA and CBI even binning Phen. Fit	+ VSA and CBI odd binning Phen. Fit	Λ -CDM Weak Priors	Λ -CDM Strong Priors	Concordance
ΔT_1	$72.2^{+3.0}_{-2.6} \mu K$	$73.9^{+2.4}_{-3.6} \mu K$	$73.5^{+2.5}_{-3.6} \mu K$	$(48 - 110) \mu K$	$(65 - 95) \mu K$	$74.9 \mu K$
ΔT_2	$45.6^{+2.5}_{-2.1} \mu K$	$43.8^{+4.4}_{-3.4} \mu K$	$46.0^{+2.5}_{-2.0} \mu K$	$(32 - 76) \mu K$	$(46 - 66) \mu K$	$53.6 \mu K$
ΔT_3	$41.5^{+4.5}_{-3.9} \mu K$	$42.6^{+3.3}_{-3.2} \mu K$	$42.8^{+4.2}_{-4.1} \mu K$	$(36 - 67) \mu K$	$(49 - 60) \mu K$	$54.6 \mu K$
ΔT_4	not constrained	$30.2^{+6.4}_{-14.0} \mu K$	$28.9^{+23.6}_{-8.6} \mu K$	$(22 - 40) \mu K$	$(26 - 37) \mu K$	$35.6 \mu K$
ΔT_5	not constrained	$27.5^{+10.1}_{-12.5} \mu K$	not constrained	$(19 - 36) \mu K$	$(22 - 32) \mu K$	$27.6 \mu K$
ℓ_1	$204^{+7.9}_{-9.5}$	$202^{+11.4}_{-4.8}$	$202^{+10.0}_{-8.1}$	192 – 279	203 – 242	215
ℓ_2	$529^{+38.7}_{-23.5}$	$518^{+27.4}_{-15.8}$	$538^{+31.7}_{-36.0}$	464 – 696	488 – 594	514
ℓ_3	$850^{+28.8}_{-42.9}$	$838^{+44.8}_{-44.8}$	$838^{+25.6}_{-37.8}$	692 – 1086	732 – 919	781
ℓ_4	$1396^{+61.4}_{-260}$	1275^{+177}_{-200}	$1254^{+33.3}_{-141}$	1140 – 1386	1210 – 1301	1190
ℓ_5	1526^{+390}_{-240}	$1351^{+547}_{-73.0}$	1604^{+205}_{-140}	1380 – 1590	1460 – 1550	1491
σ_1	$90.8^{+11.8}_{-9.3}$	$91.6^{+14.1}_{-9.7}$	$87.4^{+14.7}_{-5.1}$	86 – 136	86 – 108	93
σ_2	$112.7^{+200}_{-38.7}$	$95.1^{+51.2}_{-23.8}$	$100.6^{+200}_{-30.3}$	71 – 121	71 – 107	86
σ_3	$82.5^{+94.3}_{-37.7}$	$99.2^{+71.4}_{-24.8}$	$85.4^{+58.6}_{-44.4}$	86 – 150	86 – 150	102
σ_4	not constrained	not constrained	not constrained	70 – 120	70 – 110	87
σ_5	not constrained	not constrained	not constrained	70 – 120	75 – 110	88
ℓ_1/ℓ_2	$0.378^{+0.029}_{-0.036}$	$0.378^{+0.034}_{-0.012}$	$0.367^{+0.034}_{-0.031}$	0.379 – 0.429	0.402 – 0.422	0.418
ℓ_1/ℓ_3	$0.238^{+0.020}_{-0.019}$	$0.238^{+0.023}_{-0.012}$	$0.240^{+0.016}_{-0.019}$	0.242 – 0.290	0.259 – 0.281	0.275
$\Delta T_1/\Delta T_2$	$1.53^{+0.10}_{-0.06}$	$1.58^{+0.18}_{-0.10}$	$1.51^{+0.12}_{-0.07}$	1.23 – 1.68	1.32 – 1.51	1.40
$\Delta T_1/\Delta T_3$	$1.63^{+0.19}_{-0.15}$	$1.60^{+0.20}_{-0.08}$	$1.60^{+0.19}_{-0.16}$	1.12 – 2.13	1.26 – 1.73	1.37
$\Delta T_2/\Delta T_3$	$1.01^{+0.15}_{-0.10}$	$0.98^{+0.15}_{-0.10}$	$1.03^{+0.11}_{-0.13}$	0.80 – 1.32	0.92 – 1.17	0.98
$\ell_2 - \ell_1$	324^{+47}_{-28}	307^{+38}_{-14}	334^{+34}_{-43}	267 – 427	284 – 353	299
$\ell_3 - \ell_1$	645^{+35}_{-46}	636^{+42}_{-53}	640^{+23}_{-49}	484 – 817	528 – 679	566

with $\omega_{cdm} \sim 0.12$ and with $\omega_{cdm} = 0$ or $\omega_{cdm} > 0.3$ in disagreement with the data.

In a flat Λ -CDM model a variation in Ω_Λ shifts the spectra as $\ell \rightarrow \mathcal{R}\ell$ with the shift parameter \mathcal{R} given by (see [47], [51]):

$$\mathcal{R} = \sqrt{|\Omega_m|} \int_0^{z_{dec}} [(1 - \Omega_\Lambda)(1 + z)^3 + \Omega_\Lambda]^{-1/2} dz. \quad (5)$$

Varying the Hubble constant, parametrized as $H_0 = 100h$ Km/sec/Mpc, will change the scale of equality and will produce a similar shift. These two parameters are related to the age of the universe by:

$$t_0 = -9.8Gy \int_{inf}^0 [h^2((1 - \Omega_\Lambda)(1 + z)^3 + \Omega_\Lambda)]^{-1/2} dz \quad (6)$$

We can therefore expect that a determination of the peak positions can provide constraints on all these three quantities. In figure 7 and figure 8 we plot similar diagrams as above for $\ell_2 - \ell_1$ and $\ell_3 - \ell_1$ as functions of Ω_Λ , h and age, t_0 . As we can see, even if the region of the allowed models is quite broad because of the intrinsic degeneracies, the observed peaks positions strongly favor a model with cosmological constant $\Omega_\Lambda > 0$, a Hubble parameter $h < 0.8$, compatible with the Hubble Space Telescope (HST) result of $h = 0.72 \pm 0.08$ ([48]), and an age $t_0 > 14$ Gy, compatible with the age of the oldest globular clusters (see e.g. [49]). Again, the values obtained by the phenomenological fit are in agreement with those derived by the standard CMB+ Λ -CDM analysis.

Another parameter that affects the position of the peaks is the spectral index n_s . However, the effect is different, the shift being scale dependent. Therefore, it is better to consider the quantities ℓ_1/ℓ_2 and ℓ_1/ℓ_3 which are unaffected by the overall shift \mathcal{R} . The corresponding diagrams are plotted in figure 9. As we can see, the observed values point towards a low value of the spectral index $n_s \leq 1$.

IV. CONCLUSIONS

In this *paper* we investigated the consistency of the most recent CMB data with a class of Λ -CDM adiabatic inflationary models. First, by fitting the data with simple phenomenological functions composed by several gaussians, we have characterized the positions, amplitudes and widths of the peaks. The detection of the peaks' amplitudes and positions is quite robust and stable between different datasets. We found that all the features are consistent with those expected by the standard theory. Furthermore, we have related the features in the spectrum with several cosmological parameters by introducing cosmological diagrams that

can be used for quick, by-eye, parameter estimations. The relative amplitude of the first and second peak, in particular, of about ~ 1.54 is in agreement with the baryon density expected from BBN and suggests, in the case of negligible reionization, a value of n_s lower than one. The amplitudes of the third peak relative to the first and to the second, $\Delta T_1/\Delta T_3 \sim 1.61$ and $\Delta T_2/\Delta T_3 \sim 1$, strongly suggest the presence of cold dark matter, but limits at the same time its contribution to values $\omega_{cdm} < 0.2$. The relative position of the peaks, $\ell_2 - \ell_1 \sim 322$ and $\ell_3 - \ell_1 \sim 640$ is pointing towards the presence of a cosmological constant, a Hubble parameter on the low side of the value allowed by the recent HST measurements ($h \sim 0.65$) and, finally, to an age of the universe $t_0 \sim 14.5$ Gyrs, consistent with the measurements of the oldest globular clusters. It is moreover reassuring that all those conclusions, obtained by just drawing few lines in the diagrams presented in Figs. 5–9, are in agreement with the results obtained by a more careful standard analysis. Within the models considered in our database we found (at 68% c.l.): $n_s = 0.95 \pm 0.03$, $\omega_b = 0.022 \pm 0.003$, $\omega_{cdm} = 0.12 \pm 0.04$, $\Omega_\Lambda = 0.71 \pm 0.15$, and $t_0 = 14.7 \pm 0.7$ Gyrs.

The results obtained here show no need for modifications to the standard model, like gravity waves, quintessence, isocurvature modes, or extra-backgrounds of relativistic particles. Furthermore, possible systematic effects due, for example, to unknown foregrounds or calibration and beam uncertainties are not immediately suggested, due to the consistency between the different datasets and of the experimental data with the theory.

However, we found that the evidence for multiple oscillations is still rather weak ($\sim 2\sigma$) especially regarding the width of the peaks which is, in some cases, poorly constrained.

It will therefore be the duty of future satellite CMB experiments to point out discrepancies that might place the possibility of new physics in a more favorable light.

Acknowledgements It is a pleasure to thank Ruth Durrer, Lyman Page and Joseph Silk for useful comments. We acknowledge the use of CMBFAST [32]. CJO is supported by the Leenaards Foundation, the Acube Fund, an Isaac Newton Studentship and a Girton College Scholarship. AM is supported by PPARC.

-
- [1] E. Torbet *et al.*, *Astrophys. J.* **521** (1999) L79 [arXiv:astro-ph/9905100]; A. D. Miller *et al.*, *Astrophys. J.* **524** (1999) L1 [arXiv:astro-ph/9906421].
 - [2] P. D. Mauskopf *et al.* [Boomerang Collaboration], *Astrophys. J.* **536** (2000) L59 [arXiv:astro-ph/9911444]; A. Melchiorri *et al.* [Boomerang Collaboration], *Astrophys. J.* **536** (2000) L63 [arXiv:astro-ph/9911445].

- [3] C. B. Netterfield *et al.* [Boomerang Collaboration], arXiv:astro-ph/0104460.
- [4] N. W. Halverson *et al.*, arXiv:astro-ph/0104489.
- [5] A. T. Lee *et al.*, Astrophys. J. **561** (2001) L1 [arXiv:astro-ph/0104459].
- [6] T. J. Pearson *et al.*, astro-ph/0205388, (2002).
- [7] P. F. Scott *et al.*, astro-ph/0205380, (2002).
- [8] W. Hu, N. Sugiyama and J. Silk, Nature **386**, 37 (1997) [arXiv:astro-ph/9604166].
- [9] A. Kosowsky, M. Milosavljevic, R. Jimenez, astro-ph/0206014, (2002).
- [10] M. Kaplinghat, L. Knox, C. Skordis, astro-ph/0203413, (2002).
- [11] P. de Bernardis *et al.*, [Boomerang Collaboration], arXiv:astro-ph/0105296.
- [12] C. Pryke, N. W. Halverson, E. M. Leitch, J. Kovac, J. E. Carlstrom, W. L. Holzapfel and M. Dragovan, arXiv:astro-ph/0104490.
- [13] R. Stompor *et al.*, Astrophys. J. **561** (2001) L7 [arXiv:astro-ph/0105062].
- [14] X. Wang, M. Tegmark, M. Zaldarriaga, astro-ph/0105091.
- [15] J. L. Sievers *et al.*, astro-ph/0205387, 2002.
- [16] J. A. Rubino-Martin *et al.*, astro-ph/0205367, 2002.
- [17] S. H. Hansen *et al.*, Phys. Rev. D **65**, 023511 (2002) [arXiv:astro-ph/0105385].
- [18] A. Melchiorri and J. Silk, arXiv:astro-ph/0203200.
- [19] M. Bucher, K. Moodley and N. Turok, Phys. Rev. Lett. **87**, 191301 (2001) [arXiv:astro-ph/0012141].
- [20] L. Amendola, C. Gordon, D. Wands and M. Sasaki, Phys. Rev. Lett. **88** (2002) 211302 [arXiv:astro-ph/0107089].
- [21] R. Durrer, M. Kunz and A. Melchiorri, Phys. Rev. D **63** (2001) 081301 [arXiv:astro-ph/0010633].
- [22] F. R. Bouchet, P. Peter, A. Riazuelo and M. Sakellariadou, Phys. Rev. D **65**, 021301 (2002) [arXiv:astro-ph/0005022].
- [23] R. Dave, R. R. Caldwell, P. J. Steinhardt, astro-ph/0206372, 2002.
- [24] S. Hannestad, S. H. Hansen and F. L. Vilhane, Astropart. Phys. **16**, 137 (2001) [arXiv:astro-ph/0012009].
- [25] L. Covi and D. H. Lyth, arXiv:astro-ph/0008165.
- [26] J. Magueijo, A. Albrecht, P. Ferreira and D. Coulson, Phys. Rev. D **54**, 3727 (1996) [arXiv:astro-ph/9605047].
- [27] M. Tegmark, M. Zaldarriaga, astro-ph/0207047, (2002).
- [28] S. Hancock, G. Rocha, A. N. Lasenby & C. M. Guttierrez, MNRAS, 294, L1, 1996 [arXiv:astro-ph/9612016].
- [29] L. Knox & L. Page, Phys.Rev.Lett. **85** (2000) 1366-1369.
- [30] R. Durrer, B. Novosyadlyj, S. Apunevych, astro-ph/0111594, (2001)
- [31] S. L. Bridle, R. Crittenden, A. Melchiorri, M. P. Hobson, R. Kneissl and A. N. Lasenby, arXiv:astro-ph/0112114.
- [32] Seljak, U. & Zaldarriaga, M. 1996, Astrophys. J. , 469, 437.
- [33] A. Albrecht, D. Coulson, P. Ferreira and J. Magueijo, Phys. Rev. Lett. **76**, 1413 (1996) [arXiv:astro-ph/9505030].
- [34] F. R. Bouchet, P. Peter, A. Riazuelo and M. Sakellariadou, Phys. Rev. D **65**, 021301 (2002) [arXiv:astro-ph/0005022].
- [35] P. Binetruy and J. Silk, Phys. Rev. Lett. **87** (2001) 031102 [arXiv:astro-ph/0007452].
- [36] N. Aghanim, P. G. Castro, A. Melchiorri and J. Silk, arXiv:astro-ph/0203112.
- [37] R. Crittenden, J. R. Bond, R. L. Davis, G. Efstathiou and P. J. Steinhardt, Phys. Rev. Lett. **71**, 324 (1993) [arXiv:astro-ph/9303014].
- [38] G. Efstathiou, MNRAS, 332, 193 (2002) [arXiv:astro-ph/0109151].
- [39] A. Lewin and A. Albrecht, Phys. Rev. D **64**, 023514 (2001) [arXiv:astro-ph/9908061].
- [40] R. Trotta, A. Riazuelo and R. Durrer, Phys. Rev. Lett. **87**, 231301 (2001) [arXiv:astro-ph/0104017].
- [41] M. Douspis and P. G. Ferreira, Phys. Rev. D **65** (2002) 087302.
- [42] W. Hu, M. Fukugita, M. Zaldarriaga and M. Tegmark, Astrophys. J. **549** (2001) 669 [arXiv:astro-ph/0006436].
- [43] A. Lewis and S. Bridle, arXiv:astro-ph/0205436.
- [44] N. Christensen & R. Meyer, astro-ph/0006401, 2000.
- [45] W. H. Kinney, A. Melchiorri and A. Riotto, Phys. Rev. D **63** (2001) 023505 [arXiv:astro-ph/0007375].
- [46] L. M. Griffiths, A. Melchiorri and J. Silk, Astrophys. J. **553** (2001) L5 [arXiv:astro-ph/0101413].
- [47] G. Efstathiou & J.R. Bond [astro-ph/9807103].
- [48] W. Freedman, et al., Astrophysical Journal, 553, 2001, 47.
- [49] Salaris, M. & Weiss A., A & A, 1998, 335, 943.
- [50] M. White, Astrophys.J. 555 (2001) 88-91.
- [51] A. Melchiorri and L. M. Griffiths, arXiv:astro-ph/0011147.

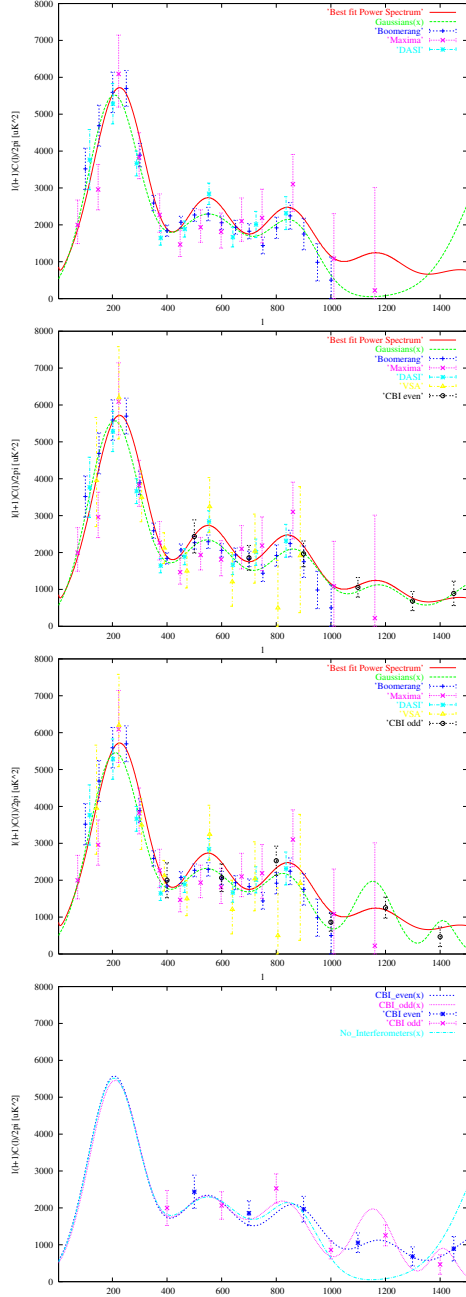


FIG. 3. First three panels: Comparison of the best-fit cosmological power spectrum and the best-fit phenomenological power spectrum for each data set (no CBI and VSA, adding VSA and CBI even binning, adding VSA and CBI odd binning). Fourth panel: Comparison of the three best-fit phenomenological power spectra. This shows their agreement until $\ell \sim 1000$. At higher multipoles, the results are very dependent on the choice of data set.

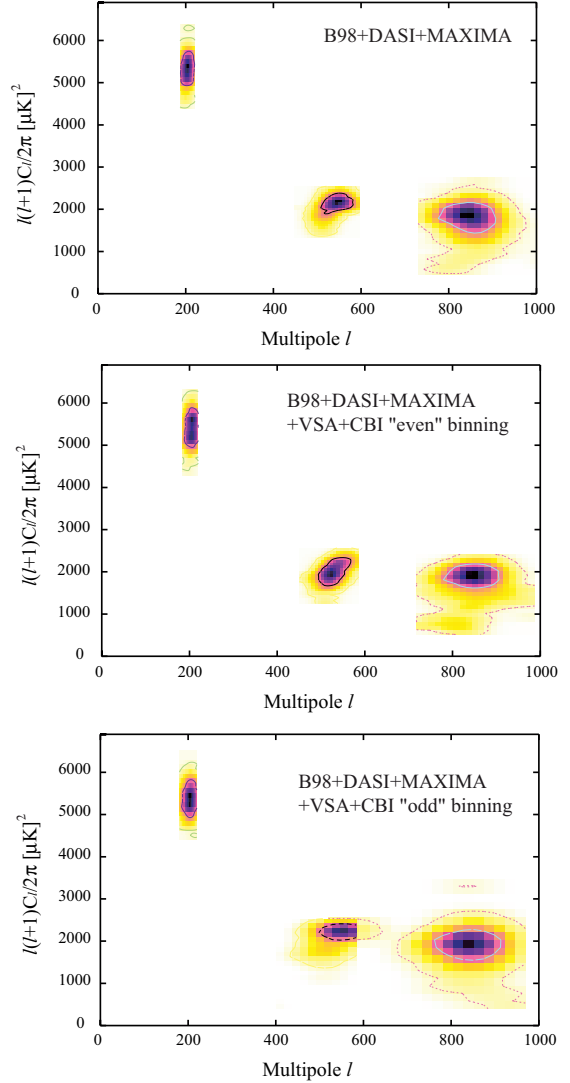


FIG. 4. 68% and 95% confidence contours in a $\Delta T^2, \ell$ plane for $(\Delta T_i, \ell_i)$ pairs, $i = 1, 2, 3$, marginalised over σ_i . The two panels are for the three different datasets analyzed: no CBI and VSA, adding VSA and CBI even binning, adding VSA and CBI odd binning. This shows the constraints on the first three peaks using our phenomenological function.

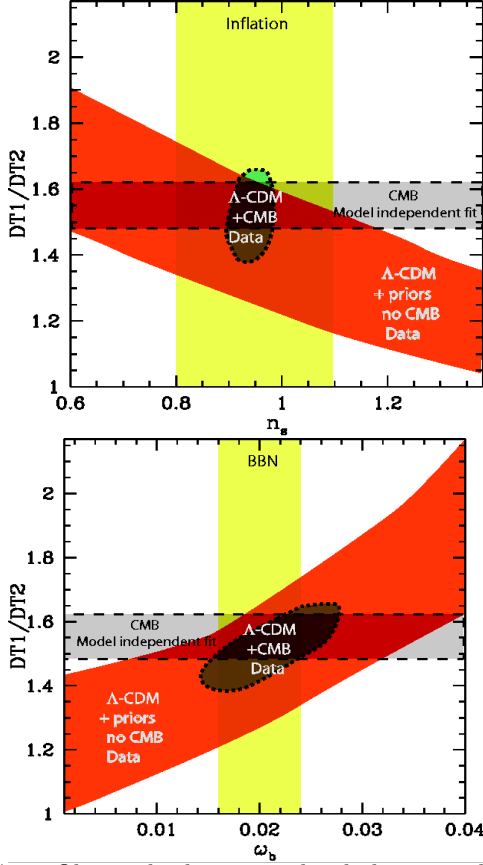


FIG. 5. Observed relative amplitude between the first and second peak and comparison with adiabatic Λ -CDM cosmological models. The red region (“ Λ -CDM no CMB”) defines all the values of $\Delta T_1/\Delta T_2$ present in the model template described in the text with the additional priors $0.1 < \Omega_{cdm} < 0.5$ and $0.55 < h < 0.88$. In the top panel, the additional prior $0.015 < \Omega_b h^2 < 0.025$ is included, while in the bottom panel we use $0.8 < n_s < 1.1$. The 68% c.l. constraint obtained by the phenomenological fit and the 95% c.l. of all the Λ -CDM models compatible with CMB are also plotted for comparison.

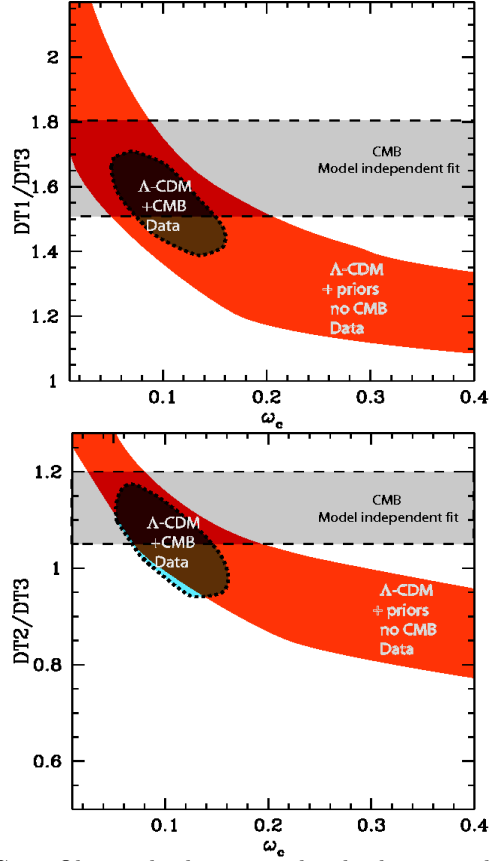


FIG. 6. Observed relative amplitudes between the first and third peaks, and between the second and third peaks, and comparison with adiabatic Λ -CDM cosmological models. The red region (“ Λ -CDM no CMB”) defines all the values of $\Delta T_1/\Delta T_3$ present in the model template described in the text with the additional priors $0.55 < h < 0.88$, $0.015 < \Omega_b h^2 < 0.025$ and $0.8 < n_s < 1.1$. The 68% c.l. constraint obtained by the phenomenological fit and the 95% c.l. of all the Λ -CDM models compatible with CMB are also plotted for comparison.

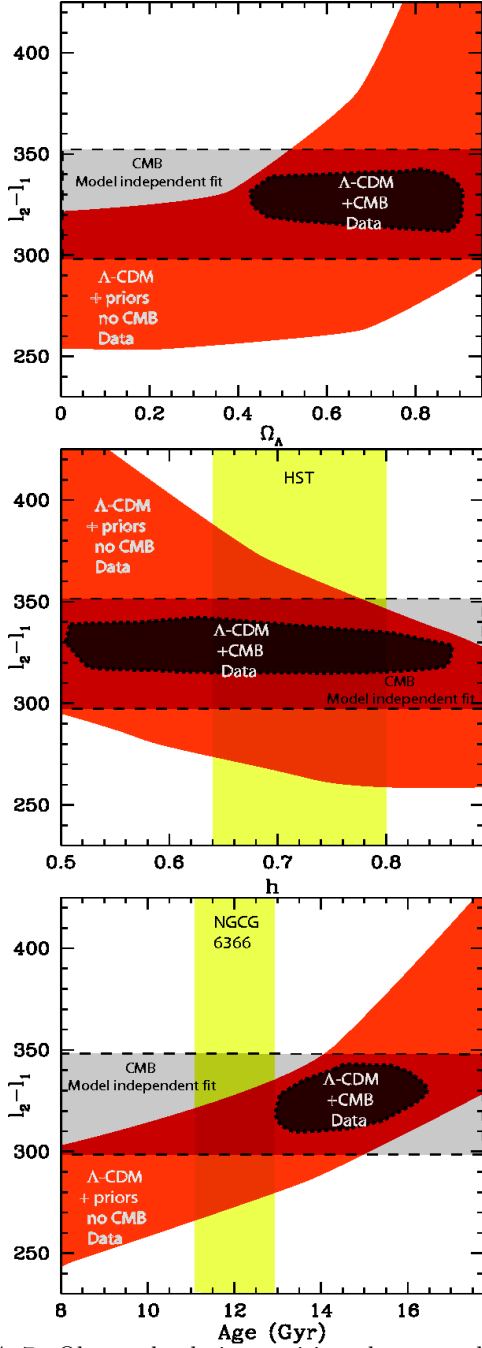


FIG. 7. Observed relative positions between the first and second peak and comparison with adiabatic Λ -CDM cosmological models. The red region (“ Λ -CDM no CMB”) defines all the values of $\ell_2 - \ell_1$ present in the model template described in the text with the additional priors $0.015 < \Omega_b h^2 < 0.025$ and $0.8 < n_s < 1.1$. In the top panel (constraints on Ω_Λ) the additional prior $0.55 < h < 0.88$ is used. In the centre panel, we use $0.1 < \Omega_{cdm} < 0.5$. The band on the y -axis on the bottom panel is the constraint on the age of the oldest halo globular cluster in the sample of Salaris and Weiss (1998). The 68% c.l. constraint obtained by the phenomenological fit and the 95% c.l. of all the Λ -CDM models compatible with CMB are also plotted for comparison.

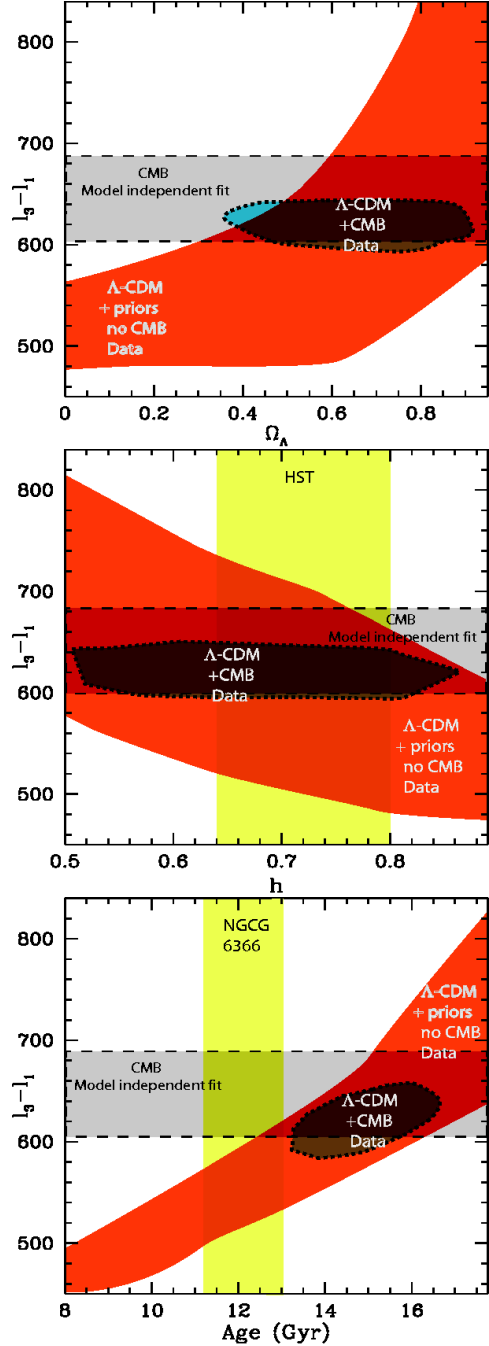


FIG. 8. Observed relative positions between the first and third peak and comparison with adiabatic Λ -CDM cosmological models. The definitions of the regions and priors used are the same as in Fig. 7

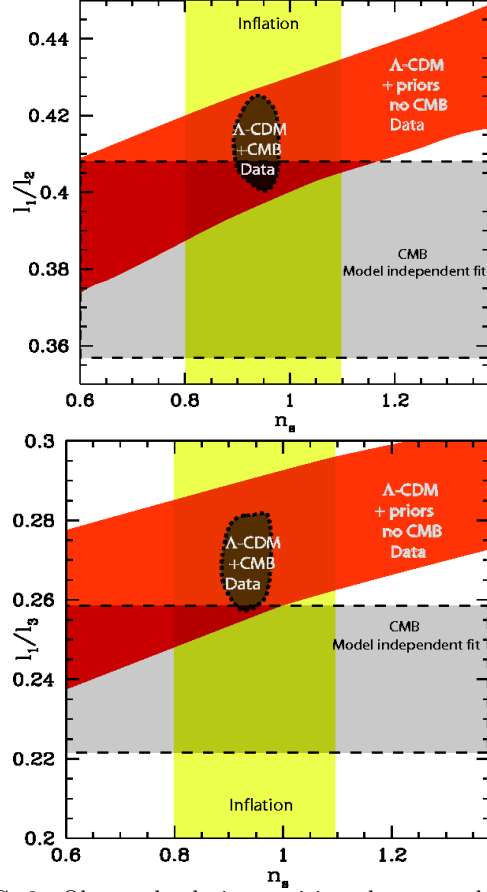


FIG. 9. Observed relative positions between the first, second and third peak and comparison with adiabatic Λ -CDM cosmological models. The red region (“ Λ -CDM no CMB”) defines all the values of ℓ_1/ℓ_2 and ℓ_1/ℓ_3 present in the model template described in the text with the additional priors $0.015 < \Omega_b h^2 < 0.025$, $0.55 < h < 0.88$ and $0.1 < \Omega_{cdm} < 0.5$. The 68% c.l. constraint obtained by the phenomenological fit and the 95% c.l. of all the $\Lambda - CDM$ models compatible with CMB are also plotted for comparison.

